GA–A23401

LARGE E×B CONVECTION NEAR THE DIVERTOR X–POINT

by
M.J. SCHAFFER, J.A. BOEDO, R.A. MOYER, T.N. CARLSTROM, and J.G. WATKINS

JULY 2000

DISCLAIMER

GA–A23401

LARGE E×B CONVECTION NEAR THE DIVERTOR X–POINT

by
M.J. SCHAFFER, J.A. BOEDO,* R.A. MOYER,* T.N. CARLSTROM, and J.G. WATKINS†

This is a preprint of a paper presented at the 14th International Conf. on Plasma Surface Interactions in Controlled Fusion Devices, May 22–26, 2000 in Rosenheim, Germany and to be published in *J. Nucl. Mater.*

*University of California, San Diego, La Jolla, California
†Sandia National Laboratories, Albuquerque, New Mexico

Work supported by
the U.S. Department of Energy under Contract Nos. DE-AC03-99ER54463, DE-AC04-94AL85000, and Grant No. DE-FG03-95ER54294

GA PROJECT 30033
JULY 2000

ABSTRACT

Electric potential, electron temperature, and electron density were measured in two dimensions (R, Z) throughout the divertor and X–point in DIII–D tokamak plasmas. An electric potential hill (~100 eV) and an associated electron pressure hill were discovered at the divertor X–point in L–mode plasmas. The potential hill extends previously reported divertor **E×B** circulation, convecting particles, energy and toroidal momentum into and out of closed magnetic surfaces and contributes significantly to transport across the boundary. The potential is explained by classical parallel (to **B**) plasma physics, when the X–point T_i is clamped lower than upstream T_i. The low X–point T_i state might be self sustaining at low heating power due to the same **E×B** circulation. We speculate that if the circulation transport is incompatible with H–mode, then the spontaneous L–H transition might require as a precondition that the X–point T_i become equalized on the near-separatrix magnetic surfaces.

Keywords: Electric potential; Electric field, **E×B** drift; plasma flow; X–point; Divertor; Divertor X–point

1. INTRODUCTION

Many tokamaks divert exhaust plasma along magnetic lines to target surfaces somewhat removed from the main plasma. The X–point, a null point of the poloidal magnetic field in conventionally diverted tokamaks, defines a separatrix, inside of which hot plasma is confined on closed toroidal magnetic surfaces. Outside the separatrix is the scrape–off layer (SOL), where plasma flows almost parallel to the magnetic field **B** along open magnetic lines to the target(s), where it deposits its energy and recombines. We restrict our attention to single–null divertors. See Fig. 1. In this paper "the divertor" is the region roughly between the X–point and the targets, and the "private region" lies between the separatrix strike points on the target. The X–point region is complex, because four plasma regions, each with distinct temperature, density and electric potential, meet there. Steep gradients and boundary layers are to be expected [1].

Parallel (to **B**) flow is clearly important in the SOL, and it has been the focus of a large body of experimental and theoretical research. Perpendicular (to **B**) flow or drift is much slower and is much less studied. We show in this paper that its consequences are far from negligible. Of special interest are effects that depend on $\mathbf{B}_T$ direction, notably the power and particle flux distributions between the inner and outer divertor targets, and the spontaneous L–mode to H–mode transition power threshold. These cannot be explained by parallel physics. We concentrate on the $\mathbf{E}\times\mathbf{B}_T$ plasma drift, because they are larger than the $\nabla\mathbf{B}$ drifts near the edge [2–4]. Of course, all flows are strongly coupled in the edge, SOL and divertor, and full understanding of their consequences requires much additional work.

We highlight measurements from DIII–D tokamak plasmas that show unexpected local maxima of potential and electron pressure close to the X–point in L–mode, for both directions of the toroidal magnetic field.

2. EXPERIMENTAL ARRANGEMENT

The experiments were performed in the DIII–D tokamak [5] with an applied toroidal magnetic field B_T = 2.0–2.1 T at radius R = 1.7 m. Both directions of B_T were employed, thereby changing the direction of B_T-dependent drifts. Neutral beam heating was used. The plasma was diverted by a single magnetic null to the lower target. Figure 1 shows a typical geometry. In most cases the X–point was located closer to the target than customary to provide diagnostic coverage above the X–point. The divertor plasma was attached to the target at the outer strike point and partially detached at the inner, which is typical in DIII–D.

Electric potential was measured by a pair of fast-stroking probe arrays, one moving vertically through the divertor region [6] and the other horizontally through the upstream SOL just below the torus equatorial plane [7]. Both probe stroke paths are indicated in Fig. 1(a). Langmuir probe tips on the arrays measured electron temperature T_e and the floating potential Φ_f. The plasma potential Φ was calculated from Φ_f and T_e as usual. Two Thomson scattering systems provided the primary measurements of T_e and electron density n_e. The divertor Thomson scattering system [8] measured at eight vertically separated locations at the same radius as the divertor probe, as shown in Fig. 1. The "upstream" Thomson scattering system [9] measured at many closely spaced points (≈ 13 mm separation) vertically across the edge and SOL, as shown in Fig. 1(a). Plasma ion temperature T_i was measured near the equator by charge exchange recombination spectroscopy (CER) [10]. No suitable T_i diagnostic covers the X–point in DIII–D.

The X–point was magnetically stepped past the divertor diagnostics, between the extremes shown in Fig. 1(b), to obtain data in two dimensions. Magnetic surfaces were calculated by the equilibrium fitting code EFIT [11]. Surfaces are labeled by their normalized poloidal magnetic flux ψ_n. $\psi_n = 1$ is the separatrix, and $\psi_n > 1$ is the SOL with ψ_n increasing outward from the separatrix. $\psi_n < 1$ is either the closed confinement or open private region with ψ_n decreasing inward from the separatrix.

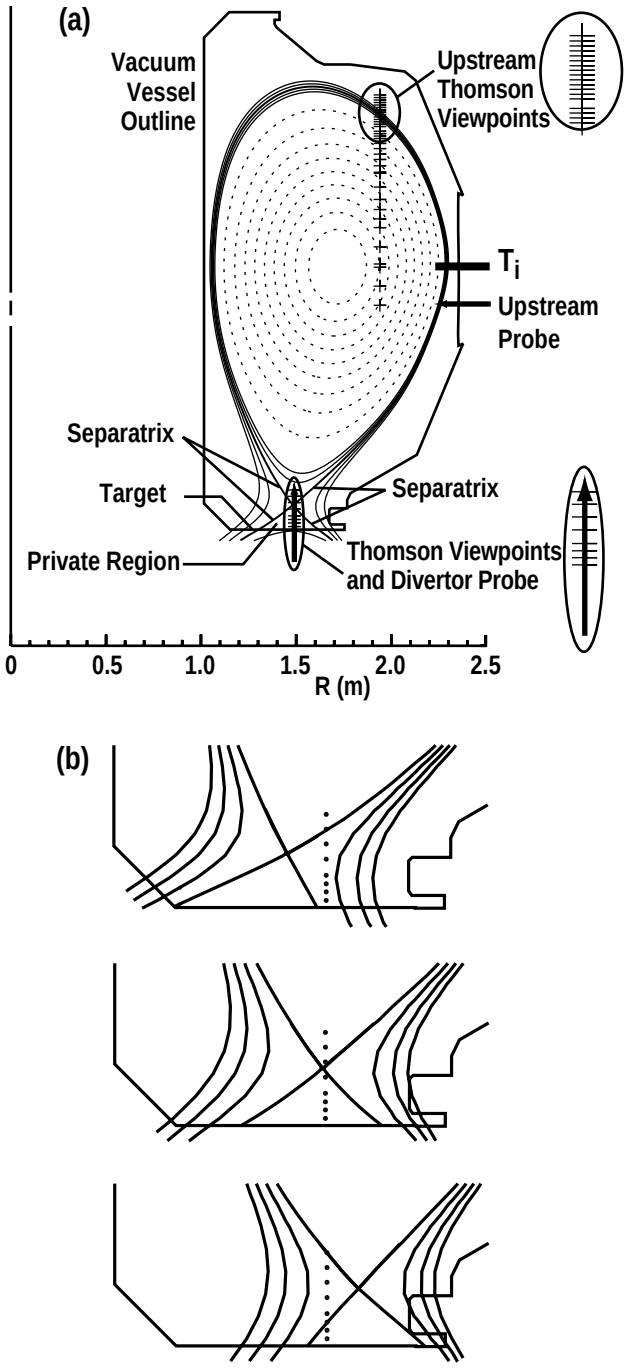

Fig. 1. (a) Single-null diverted plasma geometry shown inside the DIII–D vacuum vessel outline with the disposition of probe, Thomson scattering and ion temperature diagnostics. The 98% and 99% normalized flux surfaces are drawn inside the separatrix, and the 101% and102% surfaces outside. (b) Maximum range of divertor geometries used to measure outside and inside the X–point radius and through the X–point.

3. RESULTS

We present potential and electron pressure results from low power L–mode plasmas, which display the most interesting X–point behavior. The plasmas had I_p = 1.0 MA, line average electron density of 2.5×10^{19} m^{-3}, and were heated by 0.3 MW of neutral beam and 0.6 MW of Ohmic power. Figure 2 shows the upstream T_e and T_i profiles as functions of ψ_n. The plotted data are from a discharge with B_T directed into the page in Fig. 1 ("reversed" B_T, ion ∇B drift away from the X–point), for which we have the most complete data, but the profiles for "standard" B_T (ion ∇B drift toward the X–point) are not markedly different. Note that $T_i > T_e$ just inside and outside the equatorial separatrix, a well-known effect where the energy transport time out of the edge layer becomes less than the electron-ion energy equilibration time. We will show that the high upstream T_i is partly responsible for the X–point potential and p_e hills, whose discovery is one of the main results of this paper.

Figure 3 shows n_e, T_e and $p_e = n_e T_e$ from Thomson scattering plotted as functions of ψ_n from the same reversed B_T L–mode shot as Fig. 2. The "X–region" data cover three regions that meet at the X–point: inner SOL, outer SOL and closed or confinement surfaces. The data show that p_e near the X–point is more than 2 times greater than upstream on the same magnetic surfaces near

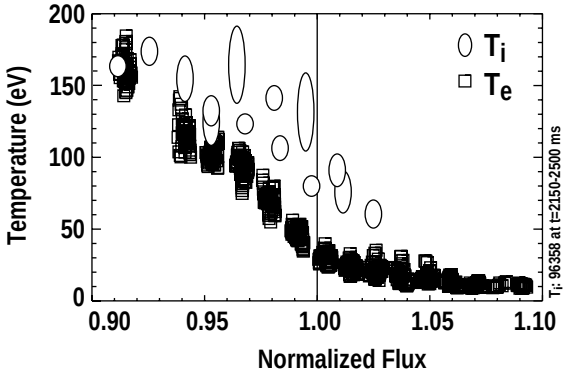

Fig. 2. Upstream ion and electron temperatures, measured by charge exchange recombination spectroscopy and Thomson scattering, respectively, as a function of ψ_n. Elliptical symbols indicate mean and standard deviation of three to five T_i measurements. The T_e time sequential data were smoothed somewhat prior to plotting for clarity.

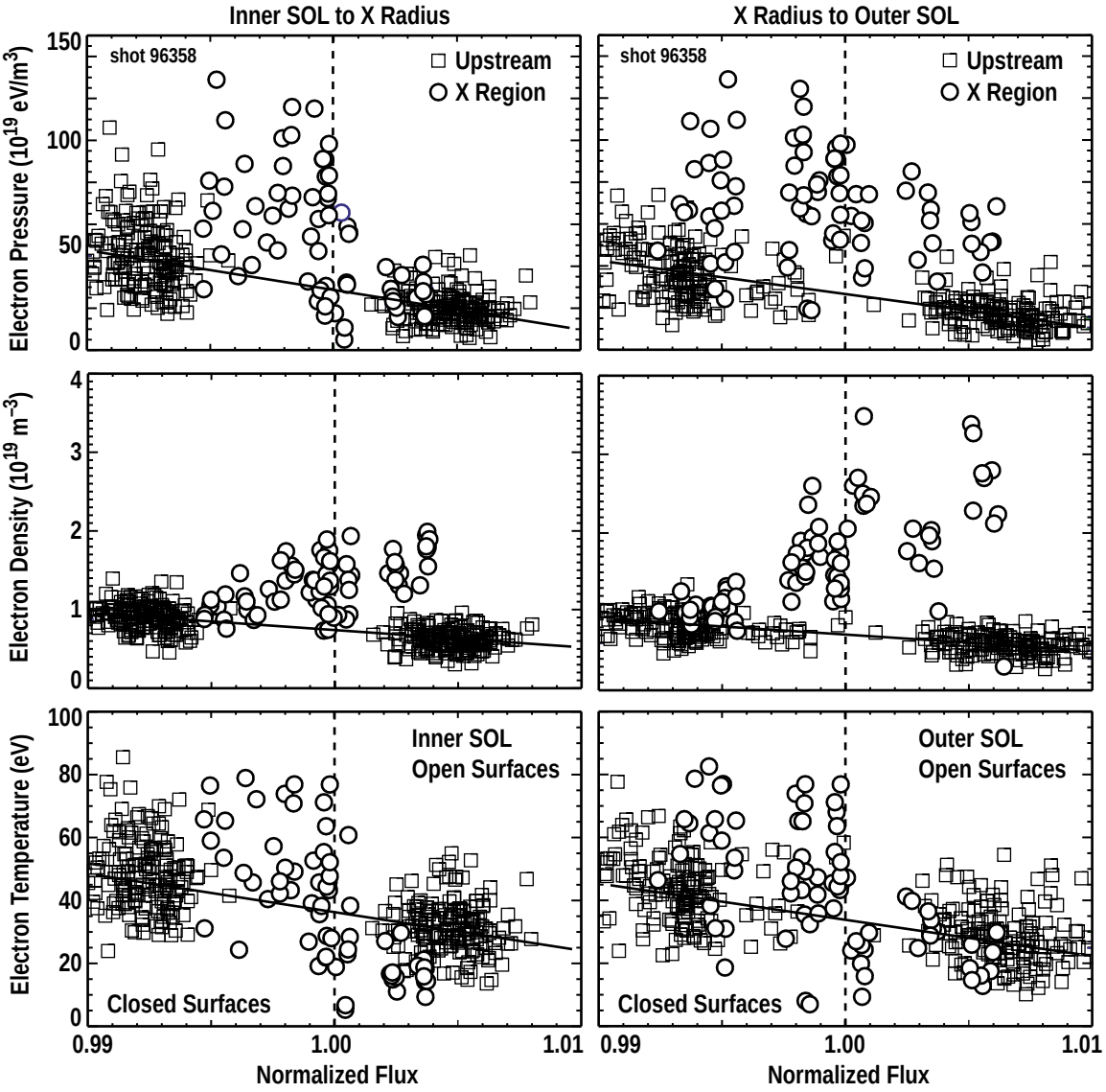

Fig. 3. Electron p_e, n_e and T_e, measured by Thomson scattering, as a function of ψ_n. Data from upstream and the X–region are distinguished by their plot symbols. X–region data are from diagnostic view points ranging from just above to just below the X–point position; data from colder plasma near the target are excluded. Left plot combines data from part of the inner SOL and through the X–point. Right plot combines data from the outer SOL and through the X–point. Data through the X–point are common to both plots. The straight lines interpolate upstream data.

the separatrix. Therefore, there is a previously unsuspected local p_e maximum or "hill" near the X–point. The excess X–point p_e is greatest on closed surfaces and the outer divertor SOL and is least on inner SOL surfaces, at least within the field of view of the diagnostic. The p_e hill is observed in L–mode with both B_T directions and in the few Ohmically heated plasmas for which we have data. The X–point maxima extend inward for about 1% of poloidal flux from the

separatrix. In contrast, p_e in H–mode remains constant on confinement surfaces (other shots, not shown). The p_e hill is not a consequence of either EFIT flux mapping or Thomson scattering errors. In these L–mode plasmas the upstream edge gradients are small, and any remaining small EFIT errors do not significantly change the upstream $p_e(\psi_n)$, etc. Near the X–point the expanded flux means that mapping divertor diagnostic coordinates to the ψ_n coordinate is very insensitive to EFIT errors. The Thomson data validity was verified, and the Thomson scattering and Langmuir probe measurements agree. The fact that the divertor and upstream density profiles in Fig. 3 merge together at about 1% of poloidal flux away from the separatrix means that there is no systematic discrepancy between the divertor and upstream Thomson density measurements. Channel-to-channel divertor Thomson scattering errors were additionally ruled out by comparison of data as the divertor geometry varied, bringing the same region of plasma successively into the view of different channels.

The p_e hill is associated mainly with a corresponding greater n_e near the X–point relative to upstream. However, as seen in the figure, T_e inside the separatrix is also locally somewhat higher near the X–point (~55 eV) than upstream (~35 eV) and contributes to the p_e hill. The higher X–point T_e is less prominent or absent with standard B_T. We do not have a satisfactory explanation for the locally higher T_e. We checked the diagnostics extensively, as discussed in the preceding paragraph. The expected jump of T_e across the X–point separatrix is clearly seen in the bottom panels of Fig. 3.

Figure 4 shows plasma potential plotted as a function of ψ_n all four X regions of the same regions of the same reversed B_T, L–mode shot as Fig. 2. Despite large fluctuations at $\lesssim$100 Hz, which are characteristic of both Φ and T_e near the L–mode separatrix [12], the near-X potentials are positive (~100 V) and much larger than the potentials upstream (~20 V) on the same magnetic surface. In shots with standard B_T the X-region potentials were similarly distributed but were ~50 V more positive, while the upstream potentials were only ~25 V more positive. A similar X–point Φ was also reported in the outer SOL and just inside the separatrix of an earlier DIII–D L–mode discharge [12], but the rest of the X–point region was not explored. We

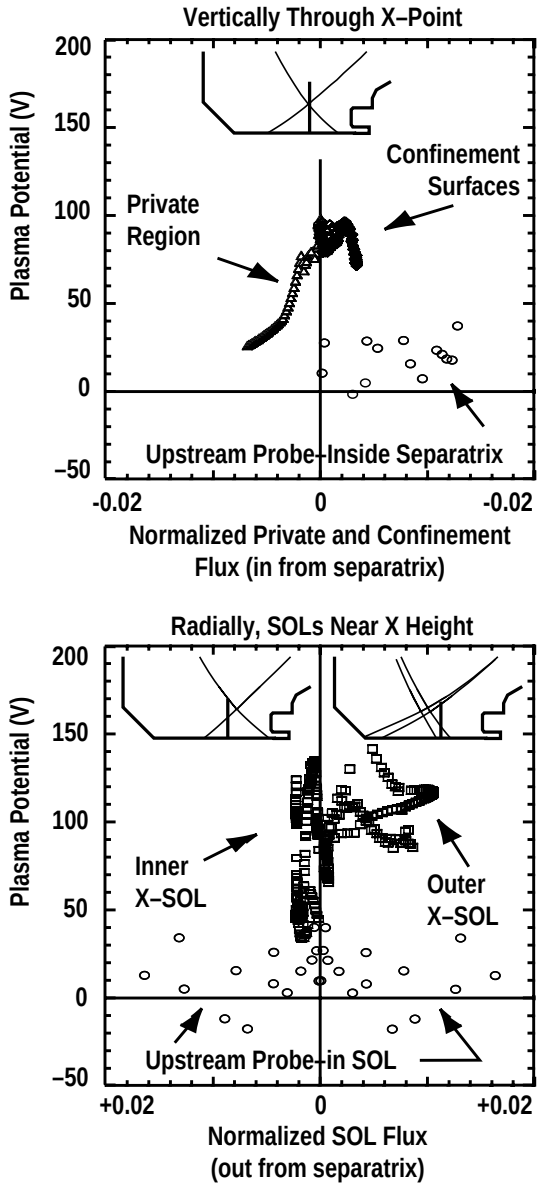

Fig. 4. Potential Φ plotted as a function of ψ_n. Target is at Φ = 0. Divertor data extend from somewhat below the X–point to somewhat above it. Upper plot shows data from a probe stroke through the private region, the X–point and into the confinement surfaces. Lower plot combines one inner SOL and two outer SOL strokes into a limited radial scan at near X–point height. Upstream data combine two strokes.

conclude that a large positive electric potential hill exists near the X–point, extending into the SOL, confinement and private flux surfaces in L–mode plasmas. The large potential difference between the X and upstream locations on closed surfaces is remarkable, because neoclassical plasma theory predicts only a weak poloidal potential variation, $e\Delta\Phi << kT_e$. In the SOL, the nonmonotonic poloidal potential variation, from target ($\Phi = 0$) to potential hill in the X–region to

a modest value upstream, is also noteworthy, because it is commonly thought, based on simplified application of the parallel plasma Ohm's law, that Φ should increase monotonically with T_e. (T_e ~5 eV at the target in these low power plasmas.) Clearly it does not.

Figure 5 shows divertor plasma potential from a standard B_T, ELMy H–mode plasma. It had I_p = 1.4 MA, line average electron density of 6×10^{19} m^{-3}, and 3.5 MW of neutral beam heating. The upstream probes have not yet reliably measured potentials inside the upstream separatrix in H–mode, because the high power density overheats the probe tip.

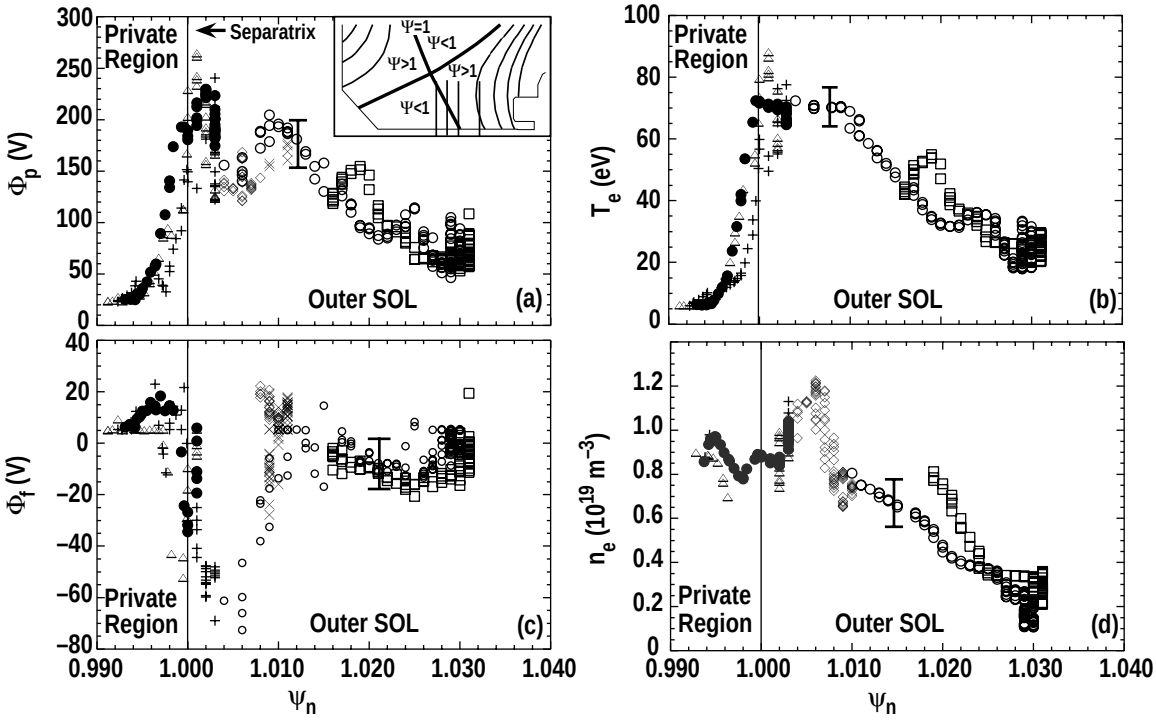

Fig. 5. Measured outer divertor profiles as a function of ψ_n, from an ELMy H–mode plasma. (a) plasma potential Φ, (b) T_e, (c) floating potential Φ_f and (d) n_e. Inset shows equivalent divertor probe trajectories schematically. Different symbols indicate different probe strokes.

4. X–POINT CIRCULATION

The electric field emanating from the potential hill drives a poloidal-like circulation on equipotentials around the X–point, sketched qualitatively in Fig. 6, at the electric drift velocity, $v_E = \mathbf{E}\times\mathbf{B}/B^2 \approx -\nabla\Phi\times\mathbf{B}_T/B_T^2$, where we use $\mathbf{B} \approx \mathbf{B}_T$ in a tokamak. The poloidal gradient causes plasma drift normal to surfaces, both closed and open. The radial potential gradient causes drift in the poloidal direction. The divertor drift, especially the drift across the private region, has been discussed theoretically [3,4] and observed experimentally [13]. The private drift was shown to be the main factor contributing to the long-observed sensitivity of the inner-outer divertor target plasma differences to the B_T direction. The newly observed potential hill on closed surfaces near the X–point, reported above, extends the circulation into the confinement volume.

The number of particles per second $\dot{N}$ convected outward by $\mathbf{v}_E$ through a ribbon surface defined by the rotation of a curve C about the major axis (see Fig. 7) and bounded by potentials Φ_1 and Φ_2 is [13]

$$\dot{N} = \int_1^2 2\pi R n \mathbf{v}_E \cdot \left(\hat{\mathbf{e}}_\phi \times d\mathbf{s}\right) \approx 2\pi \int_1^2 \frac{Rn}{B_T}(\nabla\Phi)\cdot d\mathbf{s} = 2\pi\int_{\Phi_1}^{\Phi_2}\frac{Rn}{B_T}d\Phi \quad . \tag{1}$$

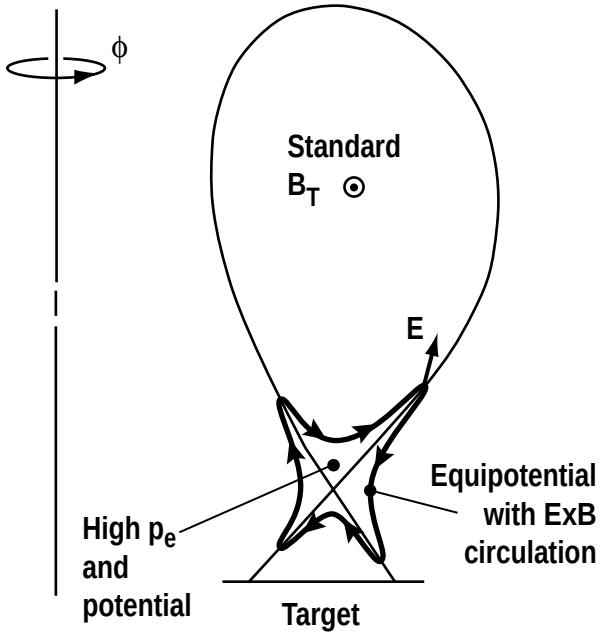

*Fig. 6. Illustration of **E×B** circulation around the X–point driven by the positive potential hill.*

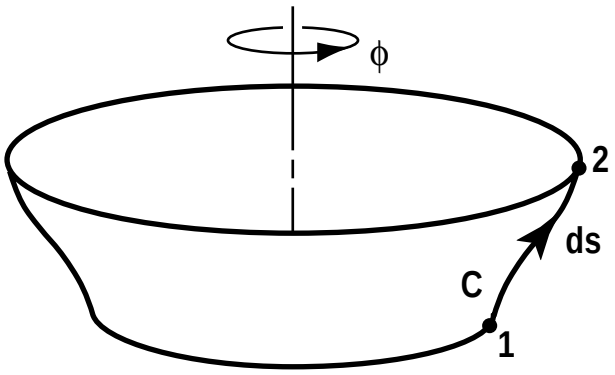

*Fig. 7. Integration path used to calculate **E×B** convection across an axisymmetric ribbon surface.*

If B_T , R and n are nearly constant across the potential gradient region, this simplifies to

$$\dot{N} \approx \left(2\pi/R_0 B_0\right)\left\langle nR^2\right\rangle\left(\Phi_1 - \Phi_2\right) \quad , \tag{2}$$

and $\dot{N}$ depends just on the potential difference across the plasma flow layer, no matter how oriented. Here $\langle\ldots\rangle$ means average along C, and B_0 is the toroidal magnetic field at some major radius R_0.

Consider first $\dot{N}$ on the private region side of the potential gradient from the ELMy H–mode data of Fig. 5. Using R_0B_0 = (1.7 m)(2.1 T) = 3.57 T·m, $\left\langle nR^2\right\rangle \approx (1\cdot10^{19}\ m^{-3})(1.6\ m)^2$ and $\Delta\Phi \approx$ 200 V yields $\dot{N} \approx 1\cdot10^{22}\ s^{-1}$, which is convected from the outer to the inner target. The measured ion flow to the inner and outer targets is $\approx 3\cdot10^{22}\ s^{-1}$, so the private $\mathbf{E}\times\mathbf{B}_T$ flow is *prima facie* important. The divertor leg potential remains positive with reversed $\mathbf{B}_T$ direction, so the $\mathbf{E}\times\mathbf{B}_T$ direction reverses with $\mathbf{B}_T$. UEDGE numerical simulation with drifts of a generic DIII–D H–mode shot predicted $\dot{N} \approx 0.7\cdot10^{22}\ s^{-1}$ [3] about the same as measured. The simulations also demonstrated that the private region $\mathbf{E}\times\mathbf{B}_T$ flow is the principal factor governing the $\mathbf{B}_T$ direction sensitivity of the power and particle flux distributions between the inner and outer divertor targets [3]. Other DIII–D divertor $\mathbf{E}\times\mathbf{B}_T$ flow results are given in Refs. [13,14]

Convection of the confined plasma across the separatrix, between the X–point and upstream, can be calculated in the same way from Eq. (2) and data in Figs. 3 and 4. Taking $n \approx 1.1\cdot10^{19}\ m^{-3}$ as the mean density between the X–point and the equator, and $\Delta\Phi$ = 65 V, yields $\dot{N} \approx 3\cdot10^{21}\ s^{-1}$.

This is more than half of the estimated cross-separatrix transport of $\sim 5 \cdot 10^{21}$ s^{-1} for this shot. The convected power P due to this circulation is calculated by replacing n by 5p/2 in Eq. (2). Taking $p \approx 195$ Pa near the X–point yields $P \approx 0.14$ MW, which is about 20% of the 0.7 MW total power crossing the separatrix. The toroidal angular momentum convected per second by the circulation across the separatrix is calculated by replacing n by $m_i n \Omega R^2$ in Eq. (2), where Ω is the toroidal rotation angular frequency. From CER measurements, $\Omega \approx 3500$ s^{-1}, so the convected angular momentum rate is about 0.14 N·m, compared with 0.165 N·m injected by the neutral beam. We do not have adequate data to do a similar calculation for poloidal angular momentum.

The X–point $\mathbf{E}\times\mathbf{B}_T$ volume exchange time is $\tau_x = |A\,B/\Delta\Phi|$, where A is the poloidal area of interest, characterizes all $\mathbf{E}\times\mathbf{B}_T$ convection. For the area bounded by the separatrix, the $\psi_n = 0.99$ surface, and extending part way upstream (this last boundary is not covered by any diagnostic and is not known), $A \approx 0.01$ m^2. Then $\tau_x \sim 0.4$ ms. It is much shorter than the ion–neutral charge exchange time, $\left(n_0 \langle \sigma_{cx} v_i \rangle\right)^{-1}$, which is $\gtrsim 3$ ms for $n_0 \lesssim 1 \cdot 10^{10}$ m^{-3}, as measured in another shot at the same density and standard B_T direction [15]. Therefore, charge exchange, which has been advanced as significant mechanism to remove plasma angular momentum [16,17], removes about an order of magnitude less angular momentum than the X–point $\mathbf{E}\times\mathbf{B}$ circulation.

5. X–POINT POTENTIAL GENERATION

We explain the L–mode X–point potential and p_e hills as a consequence of the variation of the ion pressure p_i along a magnetic flux tube wherein the total pressure $p = p_e + p_i$ remains constant. First, from Figs. 3 and 4, just inside the upstream separatrix we have $n_e \approx n_i \approx 0.75{\cdot}10^{19}$ m^{-3}, $T_e \approx 35$ eV and $p_e \approx 26{\cdot}10^{19}$ eV/m^3; $T_i \approx 125$ eV and $p_i \approx 94{\cdot}10^{19}$ eV/m^3. The total upstream pressure is $120{\cdot}10^{19}$ eV/m^3. Similarly, near the X–point separatrix we have $n_e \approx n_i \approx 1.5{\cdot}10^{19}$ m^{-3}, $T_e \approx 55$ eV and $p_e \approx 82{\cdot}10^{19}$ eV/m^3. T_i is not measured, but invoking uniformity of the total pressure, the X–point $p_i \approx 38{\cdot}10^{19}$ eV/m^3, and then X–point $T_i \approx 25$ eV. X–point p_i and T_i are much lower than upstream. The p_e hill is sustained along a magnetic flux tube by the parallel electric field. According to the parallel component of the electron momentum equation [18],

$$e\nabla_{||}\Phi = -eE_{||} = \nabla_{||}p_e/n_e + 0.71\nabla_{||}kT_e = \nabla_{||}\left(p - p_i\right)/n_e + 0.71\nabla_{||}kT_e \quad , \tag{3}$$

the potential is high where p_i is low and n_e is large, as at the X–point. Estimating $\Delta\Phi$ from Eq. (3) and the measured p_e, n_e, and T_e yields an X–point potential about 65 V higher than the upstream, which is consistent with the potential data in Fig. 4. The X–point n_e hill arises from redistribution of the plasma particles to satisfy the parallel equilibrium and does not depend on e.g. an X–point gas source.

We do not know if the potential and p_e hills and the low X–point T_i are universal features of diverted L–mode plasmas, or if they are a special case. The mechanism identified here requires that T_i be clamped to a lower value at the X–point than upstream. Classical ion parallel thermal conduction power from equator to X–point in the heterogeneous layer between the separatrix and $\psi_n = 0.995$ is small in the plasmas reported here, calculated to be ≈ 0.08 MW. Ion-electron energy exchange at ~0.01 MW is negligible, as is ion cooling to neutrals. However, convection of cool ions in across the separatrix and hot ions out by the X–point circulation can remove up to ~0.1 MW by the calculation in Section 4, if ions are much cooler in the SOL near the X–point

than on the nearby closed surfaces. This is not be implausible, because, as seen in Fig. 6, the circulation draws plasma upstream from the nearby target. Therefore, the X–point heterogeneity might be a self-consistent, self-sustaining state. Numerical modeling of a two fluid plasma with drifts and realistic X–point geometry, as in Refs. [3,4], is needed to verify whether this model is quantitatively adequate.

6. ADDITIONAL DISCUSSION

The observed absence of an X–point p_e hill in H–mode plasmas implies the absence of a potential hill and X–point circulation in H–mode. Since H–mode is characterized by a narrow edge transport barrier, we *speculate* that suppression of the X–point circulation might be important for the spontaneous L–H transition in poloidally diverted plasmas. Transition would then require homogenization of T_i on each magnetic surface, *e.g.* by exceeding a threshold heating power. Poloidal homogenization was a feature of electrode-*driven* L–H transitions in the CCT limiter tokamak [19]. The B_T direction dependence would arise from ion energy convected into or out of the heterogeneous X–point region by *e.g.* the vertical ion ∇B and curvature drift velocity, much as proposed by Hinton [20]. Further work is needed to develop and test this idea.

7. CONCLUSION

An electric potential hill and an associated electron pressure hill were discovered at the divertor X–point in L–mode plasmas. The potential hill drives a strong $\mathbf{E}\times\mathbf{B}_T$ circulation of ions across the separatrix and extends the previously reported divertor $\mathbf{E}\times\mathbf{B}_T$ circulation to closed magentic surfaces. The potential is consistent with classical parallel plasma physics, when the X–point T_i is clamped lower than the upstream T_i. The low local T_i state might be self sustaining due to the same $\mathbf{E}\times\mathbf{B}_T$ circulation. We speculate that if the circulation is incompatible with H–mode, the spontaneous L–H transition might not start until the T_i equalized on the near-separatrix magnetic surfaces.

REFERENCES

[1] F.L. Hinton, Y-B Kim, Nucl. Fusion **34** (1994) 899.

[2] A.V. Chankin *et al.*, Plasma Phys. Control. Fusion **36** (1994) 1853.

[3] T.D. Rognlien *et al.*, J. Nucl. Mater. **266–269** (1999) 654.

[4] T.D. Rognlien *et al.*, Phys. Plasmas **6** (1999) 1851.

[5] J.C. Luxon, L.G. Davis, Fusion Technol. **8** (1985) 441.

[6] J.G. Watkins *et al.*, Rev. Sci. Instrum. **68**, 373 (1997).

[7] J.G. Watkins *et al.*, Rev. Sci. Instrum. **63** (1992) 4728.

[8] T.N. Carlstrom *et al.*, Rev. Sci. Instrum. **68** (1997) 1195.

[9] T.N. Carlstrom *et al.*, Rev. Sci. Instrum. **63** (1992) 4901.

[10] P. Gohil *et al.*, Proc. 14th Symposium on Fusion Engineering, (San Diego, 1991), Vol. 2, (IEEE, New York, 1992) 1199.

[11] L.L. Lao *et al.*, Nucl. Fusion **25** (1985) 1681.

[12] R.A. Moyer *et al.*, J. Nucl. Mater. **266–269** (1999) 1145.

[13] J.A. Boedo, M.J. Schaffer *et al.*, Phys. Plasmas **7** (2000) 1075.

[14] J.A. Boedo *et al.*, Proc. 26th EPS Conf. Control. Fusion and Plasma Physics (Maastricht, 1999) ECA 23J (1999) 1185.

[15] R.J. Colchin *et al.*, Nucl. Fusion **40** (2000) 175.

[16] M.A. Mahdavi *et al.*, J. Nucl. Mater. **176–177** (1990) 32.

[17] B.A. Carreras *et al.*, Phys. Plasmas **7** (1998) 2623.

[18] S.I. Braginskii, in *Reviews of Plasma Physics*, edited by M.A. Leontovich (Consultants Bureau, New York, 1965), Vol. 1, p. 205.

[19] G.R. Tynan et al., Plasma Phys. Control. Fusion **38** (1996) 1301.

[20] F.L. Hinton, Nucl. Fusion **25** (1985) 1457.

ACKNOWLEDGEMENT

The authors acknowledge helpful discussion and contributions from D.R. Baker, B.D. Bray, K.H. Burrell, C.J. Lasnier, A.W. Leonard, G.D. Porter, and T.D. Rognlien. This work was supported by the U.S. Department of Energy under Contracts DE-AC03-99ER54463, DE-AC04-94AL85000, and Grant No. DE-FG03-95ER54294.